ELSEVIER

International Journal of Mass Spectrometry 210/211 (2001) 89–100

www.elsevier.com/locate/ijms

A 20 kV orthogonal acceleration time-of-flight mass spectrometer for matrix-assisted laser desorption/ionization

D.S. Selby, V. Mlynski, M. Guilhaus*

School of Chemistry, The University of New South Wales, Sydney 2052 Australia

Received 27 December 2000; accepted 21 March 2001

Abstract

A compact time-of-flight mass spectrometer has been constructed with the reflecting analyzer region orientated to be orthogonal to the desorption axis of a matrix-assisted laser desorption/ionization source. The instrument is designed with a detector that is large enough to accommodate a correspondingly large desorption velocity spread without the need for collisional cooling. Laser desorbed positive ions from a positively biased probe enter a field free fill region of an orthogonal accelerator, initially at ground potential. The ions are then orthogonally accelerated to reach a final potential of −20 kV and a kinetic energy of ~21 keV. The space focus of the reflectron geometry is adjusted to lie in the ion mirror to allow easy conversion to the linear mode. The detector of the current configuration is a 70 mm diameter microsphere plate. The spectrometer has a total length of less than 1 m and, in good agreement with simulations, it provides a typical resolution of 8000 (full-width at half-maximum). Detection limits determined with ~10–50 laser shots were in the low femtomole range up to $m/z \sim 10000$. Beyond this limit, sensitivity appears to be lowered by decreasing detector efficiency and the increasing velocity spread of the desorbed ions. Mass calibration of the instrument is very simple and reproducible. Measured mass accuracy with external calibration is better than 100 ppm over several days. Limitations in mass accuracy are attributed to the drift of the power supplies and timing jitter. A focusing method for improving high mass sensitivity by a factor of typically 20 is briefly described and demonstrated with the detection of molecular ions of myoglobin ($m/z \sim 17000$). (Int J Mass Spectrom 210/211 (2001) 89–100) © 2001 Elsevier Science B.V.

Keywords: Time-of-flight; MALDI; Orthogonal acceleration

1. Introduction

Over the last decade, orthogonal acceleration (oa) time-of-flight mass spectrometry (TOFMS) has established itself as the method of choice for the coupling of continuous ionization sources with the TOF mass analyzer [1,2]. Several advantages are inherent in this configuration including: the efficient sampling of ions in the ion beam, the removal or minimization of the limiting effects of the ion source energy spread on resolution, and very good mass accuracy and stability of mass calibration as a result of the ions having a zero initial velocity component in the time-of-flight direction [3,4]. In effect, the source and analyser operate more independently in the oa-TOF configuration than in conventional "in-line" TOF systems.

Matrix-assisted laser desorption/ionization (MALDI) [5] is a pulsed ion source that is commonly used with

* Corresponding author. E-mail: m.guilhaus@unsw.edu.au

Dedicated to Professor Nico Nibbering on the occasion of his retirement.

conventional TOF mass analyzers. Previous attempts to obtain oa-TOF advantages with MALDI indicated that the source and mass analyzer were substantially decoupled [6,7]. The resolution, mass calibration stability, and mass accuracy were relatively unaffected by the large variations in desorption velocities resulting from the use of different matrices and laser powers. This is a relative advantage compared to conventional delayed extraction MALDI systems [8,9] where calibration and mass accuracy are affected by the conditions in the source and some form of internal calibration is usually required. The main disadvantage apparent in the early MALDI oa-TOF combinations was poor sensitivity at high *m/z*. This may be attributed to two main factors. First the use of relatively low ion kinetic energies limits the detector efficiency at high *m/z* [10,11]. Second the kinetic energy spread increases with *m/z*. This brings about (for ions having the same *m/z*) a corresponding increase in the average ion velocity and velocity spread, observed parallel to the plane of the detector. The resulting divergence of drift trajectories thus contributes to a further decrease in detection efficiencies at high *m/z* when ions, at the extremes of the velocity spread, no longer strike the active area of the detector.

The development of hybrid quadrupole TOFMS systems [1,2,12,13] has demonstrated the ability of radio frequency multipole collision cells to cool and focus ion beams from electrospray sources [14]. Collisional cooling has also been applied with ions produced by MALDI to create a pseudocontinuous ion beam with a narrow energy spread [15]. This approach, when used with quadrupole-TOF hybrid instruments has an additional important advantage. Mass selection in the quadrupole prior to collisional dissociation and mass analysis of fragment ions in a TOF mass analyzer allows tandem mass spectrometry (MS/MS) to be undertaken for MALDI generated ions. However this arrangement is quite complex and the mass range of the TOF stage for singly charged ion remains limited, when relatively low ion kinetic energies are used. The use of collisional focusing may also lead to unwanted fragmentation of molecular ions.

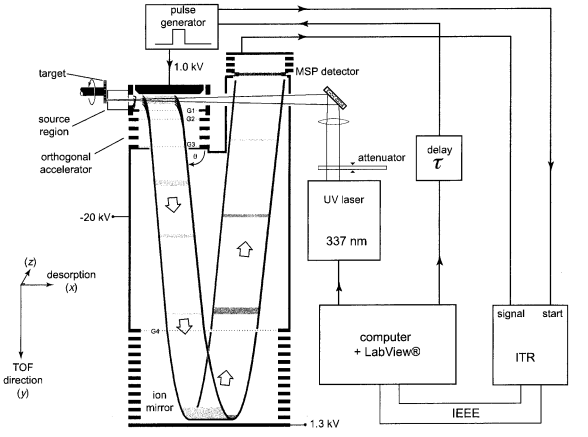

Fig. 1. Schematic arrangement of the instrument described in this article. G1–G4 are grids. The z axis is normal to the plane of the page. Detailed specifications are given in Table 1.

The instrument described in this article was developed to improve the design of our first MALDI oa-TOF system [7] without resorting to collisional cooling and its associated apparatus (differential vacuum system, radio frequency multipole, and collision cell). The aim of the instrument was to provide basic mass analysis with simplified calibration requirements and reliable mass accuracy. The main departure from the earlier device lies in a higher ion kinetic energy in the TOF mass analyzer, more typical of conventional MALDI instruments, and the use of a larger detector. Additional improvements involve the use of customized high transmission grids with rectangular repeat cells [16,17] and a biased probe potential to adjust the average velocity of ions in the desorption axis of the MALDI source.

2. Experiment

2.1. Apparatus

A schematic diagram of the mass spectrometer is shown in Fig. 1 and critical instrument parameters are listed in Table 1. The source region (probe and lens assemblies) was powered by a Tennelec TC945 high voltage power supply (Canberra Industries, Meriden, CT). The push-out plate and mirror backplate utilized

Table 1
Instrument specifications

MALDI source	
Laser and optics	337 nm nitrogen laser, 100 μm diameter spot size, normal incidence with target
Distance target to oa axis	73 mm
Aperture	2 mm wide at 25 mm from target
Probe bias	0–200 V
Distance target to lens aperture	1.0 mm
Lens aperture diameter	1.0 mm
Orthogonal accelerator	
Pushout pulse delay	3–200 μs programmable relative to laser firing
Pushout pulse amplitude	1005 V (~60 ns rise time)
Axis of ion source	1.25 mm from pushout plate
1st acceleration gap	5.35 mm ($E = -186$ V/mm)
2nd acceleration gap	5.50 mm ($E = -225$ V/mm)
3rd acceleration gap	40.0 mm ($E = -468$ V/mm)
Grid material	12 lpc × 120 lpc Ni, 70% transmission each, 5–10 μm thick
Grid support & field rings	77 mm outer diameter 48 mm inner diameter
Drift regions and chamber	
	550 mm (forward), 619 mm (reflected), −20 kV potential
	900 mm × 300 mm precision machined aluminium chamber,
	240 L s^{-1} turbomolecular pump, 1×10^{-6} mbar working pressure
Ion mirror	
Deceleration gap	158 mm ($E = 135$ V/mm)
Grid material	4 lpc × 40 lpc stainless steel, 80% transmission
Grid support & field frames	250 mm (x) × 125 mm (y) outer dimensions,
	210 mm × 85 mm inner dimensions
Detector and digitizer	
	70 mm (diameter) micro sphere plate,[a] centred
	205 mm from accelerator axis
	4 Gsample/s × 1 GHz DSO[b]

[a] Single thickness plate with measured pulse width 800 ps in customised assembly with anode operating at ground potential. Plate supplied by El-Mul Technologies (Yavne 81104, Israel).
[b] LeCroy 9384 with PP094 Adapter (LeCroy Corporation, New York).

separate +1.5 kV MK series supplies (Glassman High Voltage, Salem Industrial Park, NJ). Grid 1 was connected to a custom-built power supply. All other grids and the front of the detector were connected to a −25 kV MK series supply, from Glassman High Voltage. A more detailed description of the components follows.

The ion source was similar to that of an earlier prototype instrument [7], with two important modifications. First, a potential was applied to the probe in some experiments (typically in the range from 150 to 195 V) to adjust the desorption energy and increase the number of ions that reached the detector. Second, a lens was installed in the source region to redirect ions toward the entrance slit of the orthogonal accelerator and thereby increased sensitivity. A positive potential was applied to the lens (from +40 to +150 V), when required, to direct more ions through the 2 mm (wide) × 14 mm high slit, located 25 mm after the entrance to the lens assembly. The distance between the target surface and the entrance aperture of the lens assembly was 1.0 mm. Samples were inserted and removed through a ball valve and vacuum lock. A modified lens was used in a preliminary attempt to extend the mass range to $m/z \sim 20000$ [18]. It provided focusing of the ion's position in the

TOF axis and velocity adjustment in the desorption axis, by applying a potential (typically in the range 40–200 V) after a short delay (2–20 μs).

A 337 nm UV laser was used with the same optical arrangement as described for the earlier prototype instrument [7]. The laser beam was directed along the desorption axis, through the orthogonal accelerator and had a 90° incidence angle with the target. The observed desorption craters had a diameter of $\sim$100 μm.

The orthogonal accelerator consists of a push-out electrode and three grids, with voltages set to define three acceleration regions when the pushout plate is pulsed to $\sim$1 kV, as indicated in Table 1. The pulse driver circuit was custom made in our laboratory. The grids were lithographically mastered for the instrument and they consist of 120 $\times$ 12 lines per cm nickel grid made by electodeposition (Buckbee Mears, St Paul, MN). These grids were designed to improve transmission and resolution relative to typical grids with square repeat cells. The rectangular repeat cells of this mesh were aligned with the longer dimension parallel to the desorption axis of the ion source. A detailed discussion of the grids has been published elsewhere [16,17].

The acceleration regions are adjusted to bring the spatial focus to a point inside the ion mirror. This unconventional configuration allows easy conversion of conditions to linear TOFMS (the detector for the linear TOF configuration has not yet been installed).

The drift region was enclosed in a liner that was floated at $-$20 kV for most experiments. This potential was divided down by way of resistor chains on the orthogonal accelerator grid assembly and the ion mirror to provide the required electric fields in these devices. The first grid was biased at 2.5 V to null the effects of field penetration so that the first acceleration gap was essentially field free when ions were entering it.

The rectangular ion mirror assembly uses a high transmission stainless steel rectangular repeat-cell grid mastered for this instrument by Towne Technologies (Somerville, NJ). The grid was aligned similarly to those in the orthogonal accelerator. Eleven spacer frames are used to create a constant field between the mirror mesh, held at the accelerating potential, and the back plate, which was set to a higher potential than the push-out pulse.

The detector assembly was installed on the same mounting plate as the orthogonal accelerator. It consists of a 70 mm diameter El-Mul (Yavne, Israel) single thickness microsphere plate (MSP) electron multiplier [19], followed by field spacer rings (to step the potential down to ground) and a collector plate for the emitted electrons. Charge arriving on the collector plate was measured as a transient voltage on LeCroy 9384 (LeCroy Corporation, Chestnut Ridge, NY) integrating transient recorder (ITR). The bias potential across the MSP was adjusted with an external resistor chain and could be set to 2.94 or 3.14 kV, when the liner potential was $-$20 kV. A more detailed description of the detector assembly and its performance characteristics will be published separately.

2.2. Instrument control and data acquisition

Instrument control and data acquisition were coordinated by a personal computer running an integrated set of custom designed modules (virtual instruments) in the LABVIEW (National Instruments, Austin, TX) programming environment. One virtual instrument (VI) set the potentials of the critical power supplies, whereas another controlled the laser firing and delay (τ in Fig. 1) between laser firing and triggering the orthogonal accelerator's push-out pulse. A further VI was used for communicating with the ITR by way of an IEEE (GPIB) interface so that data acquisition could be initiated from the keyboard and full spectral data could be downloaded during experiments. This VI also provided for mass calibration and display of spectra on a *m/z* axis with two internal calibration marker peaks in the TOF spectrum. Alternatively external calibration could be used with previously determined constants. Integration of cursor-selected peak areas was included in the functions of the data system. Spectra were exported in formats suitable for further display and analysis using commercially available software.

2.3. Simulation of instrument performance

A customized program (SIMTOF) has been written to predict peak shapes in TOFMS based on ion starting parameters and instrument specifications. In addition to the ion starting parameters, this can take into account the effect of grids and the temporal response of the detector. Independent calculations using probability density functions [20] and Monte Carlo algorithms are provided in this program. A full description of this program will be published separately.

2.4. Sample preparation and introduction

The matrix used in these experiments was 2,5-dihydroxybenzoic acid (Sigma Chemical Co., St Louis, MO). Samples of 5,10,15,20-tetraphenyl-21H,23H-porphine, gramacidin S, and a mixture of C_{60}/C_{70} were obtained with unspecified origin, but were determined to be pure by mass spectrometry. Bee venom melittin (Sigma), oxidised bovine insulin chain B (Fluka, Chime AG CH-9471, Buchs) and bovine insulin (Sigma) were purchased and also used as analytes. All samples were dissolved in 1:1 (v/v) acetonitrile and 0.5% aqueous trifluoroacetic acid, except for porphine which was dissolved in 1,2-dichloroethane.

Samples were prepared by the dried droplet method, where matrix (10 mg/mL) and analyte (1–4 mg/mL) were sequentially applied to the sample slide, with rapid drying under an infrared lamp between applications. 2 μL of analyte was applied, with a volume of matrix which gave an approximately 1000-fold molar excess of matrix. The C_{60}/C_{70} sample was run neat and thus served as its own matrix.

Delay times (τ) between laser firing and triggering of the push out pulse were varied between 3 and 50 μs across the mass range. This delay was necessary to allow ions to traverse the distance between the MALDI target and the orthogonal accelerator. Ions traveling parallel to the desorption axis required an average energy of 242 eV. Ions with this energy were displaced (in the desorption axis) from the centre of the orthogonal accelerator to the centre of the detector during their time-of-flight through the mass analyzer. Some energy was provided by the MALDI process and the rest was given by a bias potential of between 150 and 195 V applied to the sample probe. The settings of the delay τ and the probe bias will be discussed more fully later in this article, in relation to the range of *m/z* transmitted to the detector.

3. Results and discussion

3.1. Mass spectra, resolution, and grid orientation

Typical spectra are shown for standard compounds in Figs. 2 and 3. Fig. 4 is a graph of the observed peak-width squared versus *m/z*. The square of the peak-width $(\delta t)^2$ is expected to increase linearly with (*m/z*) in TOF mass spectra [21,22]. The width arises from the spread of arrival time and the temporal characteristics of the detector and timing electronics (detector pulse width and jitter) [21]. The graph allows the temporal contribution of the detector and timing jitter to be separated from the arrival time contribution as originally explained [21]. Thus, from the data presented, an overall resolution of about 8000 FWHM is apparent from the slope of the graph, whereas the intercept indicates a detector pulse and jitter contribution of about 1.2 ns. The points that lie furthest from the line correspond to spectra obtained with the maximum [larger $(\delta t)^2$] and minimum [smaller $(\delta t)^2$] number of shots required to obtain a good signal-to-noise ratio. The most probable explanation for the larger than usual scatter on this graph is that there was an increasing jitter contribution resulting as the number of shots accumulated increased. However, the trend of the graph is a good measure of the overall performance of the instrument. Simulations of peak shape (SIMTOF program) were performed with the instrumental parameters in Table 1 and the ion parameters in Table 2. These predicted that the instrument should have given a theoretical resolution of ~8000 [as shown in Fig. 2(b)]. This, however, required that the value for the mass-dependent velocity spread in the TOF direction (considered in isolation from velocity in all other directions) corresponded to a constant ±3 meV kinetic energy spread. The corresponding divergence (±0.2°) in the desorbing plume

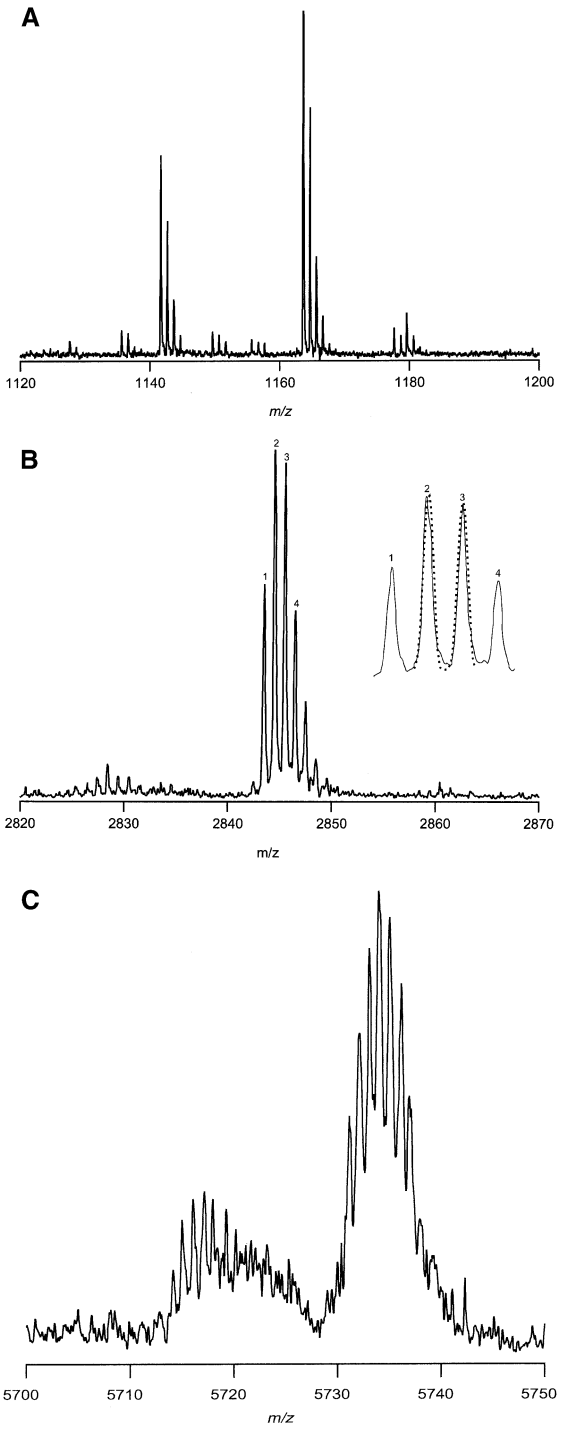

Fig. 2. Typical MALDI mass spectra obtained for (a) gramacidin S, (b) melittin, and (c) insulin. A resolution of ~8000 is apparent. The inset in the melittin spectrum shows the molecular ion region expanded and a SimTOF simulation of the peak shape (see text).

is much less than expected from geometric restrictions on the divergence (±1°) as imposed by the slit. The observed resolution could not have been obtained with the latter divergence if the initial velocities (TOF direction) in the accelerator had been uncorrelated with the initial positions of ions in the TOF axis. The observed resolution could be explained if some position-velocity correlation exists or if collisions during the desorption process decrease the divergence of the plume as suggested recently [23]. This issue is the subject of further investigations.

The resolution of orthogonal acceleration TOFMS instruments may be affected by dispersion of ions near grids and particularly by "wires" that are at right angles to desorption velocity. The instrument constructed in this study incorporates grids designed specifically to minimize these dispersions. Instead of square repeat cells, rectangular cells were created by having ten times as many wires per unit length parallel with the desorption direction than at right angles to it. This effect was illustrated by rotating the grids of the orthogonal accelerator 90° from the optimum theoretical orientation. The resolution as measured by the above-mentioned procedure was reduced from 8000 to ~4800 FWHM after rotation. Full details of this effect have been published recently [16,17].

Fig. 3. shows the MALDI spectrum of C_{60}/C_{70} obtained with a laser energy well above threshold. Near-threshold laser power resulted in spectra showing only C^{+}_{60} C^{+}_{70} ions. It is apparent that the ionization of this compound with high laser power generated carbon cluster ions over a wide mass range. Peaks were observed at every 24 Da (i.e. C_2 units) with abundance diminishing at *m/z*~5000. It is apparent that ions over a wide *m/z* range were transmitted by the instrument.

3.2. Calibration and mass accuracy

Calibration relationships between the measured time-of-flight and the known accurate *m/z* of the observed ions are very linear in oa-TOFMS [1]. In the mass calibration used to measure the mass accuracy of the instrument, 46 individual TOF measurements were made from a distribution of ions from gramici-

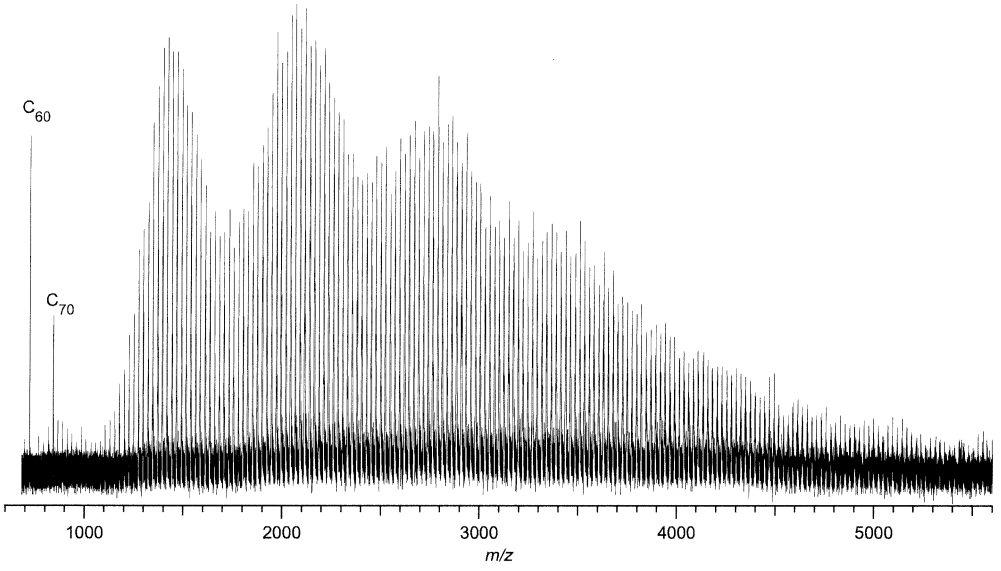

Fig. 3. MALDI mass spectrum obtained from a sample of C_{60}. Carbon cluster ions with a wide range of *m/z* are transmitted by the instrument. The sample is acting as its own matrix.

din S, melittin, insulin chain B, insulin, ubiquitin (total *m/z* range from 1141.7 to 8587.9). A linear fit to the flight-time versus $(m/z)^{0.5}$ gave an R^2 value of 0.999 999 979. The analysis of residuals from this set of data gave a normal distribution of mass errors with an average of −4.2 ppm, a standard deviation of 53 ppm and an rms error of 52 ppm. This precision was consistent with the combined effects of a 20 ppm measured power-supply drift, the drift in the trigger delay (e.g. a 30 ppm mass error for melittin) and the

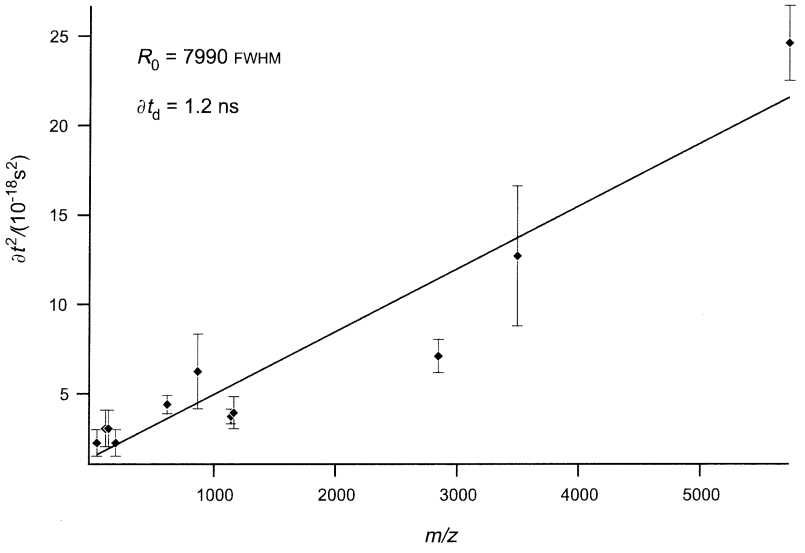

Fig. 4. Variation of the square of peak width with *m/z*. This graph indicates the contribution of constant temporal sources of peak broadening as well as the ultimate resolution (i.e. with a jitter free detection system and a zero width detector pulse).

Table 2
Ion parameters and instrument parameters[a] taken into account in modeling of peak shapes in the SIMTOF program

Velocity spread in TOF direction[b]	±1 meV standard deviation truncated at ±3meV
Spatial spread in TOF direction[c]	1 mm standard deviation truncated at ± 1 mm
Energy dispersion on grids[d]	0
Detector temporal spread and jitter ns	1.2 ns FWHM Gaussian signature

[a] Instrumental parameters are in addition to those shown in Table 1.
[b] The velocity spread is generated to be Gaussian. It has a standard deviation and truncation limits, corresponding to the kinetic energy values given, if the velocity in other directions is ignored.
[c] Limited by entrance aperture to orthogonal accelerator.
[d] Not significant with rectangular grid cells.

Table 3
Probe bias parameters

	Desorption velocity and kinetic energy[a]		Bias required to raise PKE_{des} to 242 eV
m/z	u_{des} (ms^{-1})[b]	PKE_{des} (eV)[a]	
100	4000	8.3	233
500	2000	10.4	232
1 000	1500	11.7	230
5 000	1000	25.9	216
10 000	1000	51.8	190
20 000	1000	104	138
50 000	1000	259	−17

[a] PKE refers to the partial kinetic energy calculated on the basis of the component of velocity in the desorption direction [16,17].
[b] From direct measurements with linear MALDI oa-TOF [7] see text.

uncertainty in identification of the peak centroid resulting from noise and the finite digitizer frequency (typically 30–60 ppm for melittin). These uncorrelated errors would add in quadrature to ~50–75 ppm.

When the mass calibration previously described was applied to spectra collected over several days, the worst case averaged mass error was ~100 ppm with a precision of ~70 ppm.

3.3. Desorption velocity and role of τ delay and probe bias potential

A positive potential was applied to the target to create an accelerating field in the vicinity of the desorbing ions. The velocity of desorbing MALDI ions was adjusted so that ions reaching the axis of the orthogonal accelerator after a delay of τ would, during their subsequent time-of-flight through the TOF analyzer, be displaced (in the desorption direction) to the axis of the detector. Desorption velocities expected prior to acceleration were estimated with data from a linear MALDI oa-TOF instrument [7] and published values [23–26] (see Table 3). The linear instrument allowed the angle of the drift tube to be adjusted so that the distribution of desorption velocity could be observed for ions of different mass and with various matrix and laser power combinations. The results on the prototype instrument were in good agreement with other studies where the velocity of ions was observed at some distance from the probe [23,24,26]. These velocities are systematically higher than desorption velocity estimates in delayed extraction systems [27]. This has been attributed to the fact that the orthogonal acceleration geometry selects a population of ions with small velocity components normal to the desorption axis. Fig. 5(a) plots the delay required for an ion with adjusted desorption velocity to travel from the target to the axis of the orthogonal accelerator. Ions selected at delays outside the area defined by the limit lines will not reach the detector. Fig. 5(b) is a similar diagram for allowable conditions for the probe bias potential. A relatively wide range of mass around an optimum mass is clearly transmitted to the detector (see Fig. 3). This may be attributed to the size of the grids of the orthogonal accelerator compared to the distance to the target as well as the size of the detector. Experimentally determined values of τ and the bias were observed to be approximately in agreement with the predictions of Fig. 5.

3.4. Estimation of sensitivity

Sensitivity estimates for compounds in the range of *m/z* 1200–17 000 are given in Table 4. The estimate is based on the amount of sample that was consumed in routine experiments. The known amount of sample deposited in the spot was assumed to be uniformly distributed. The amount desorbed was determined

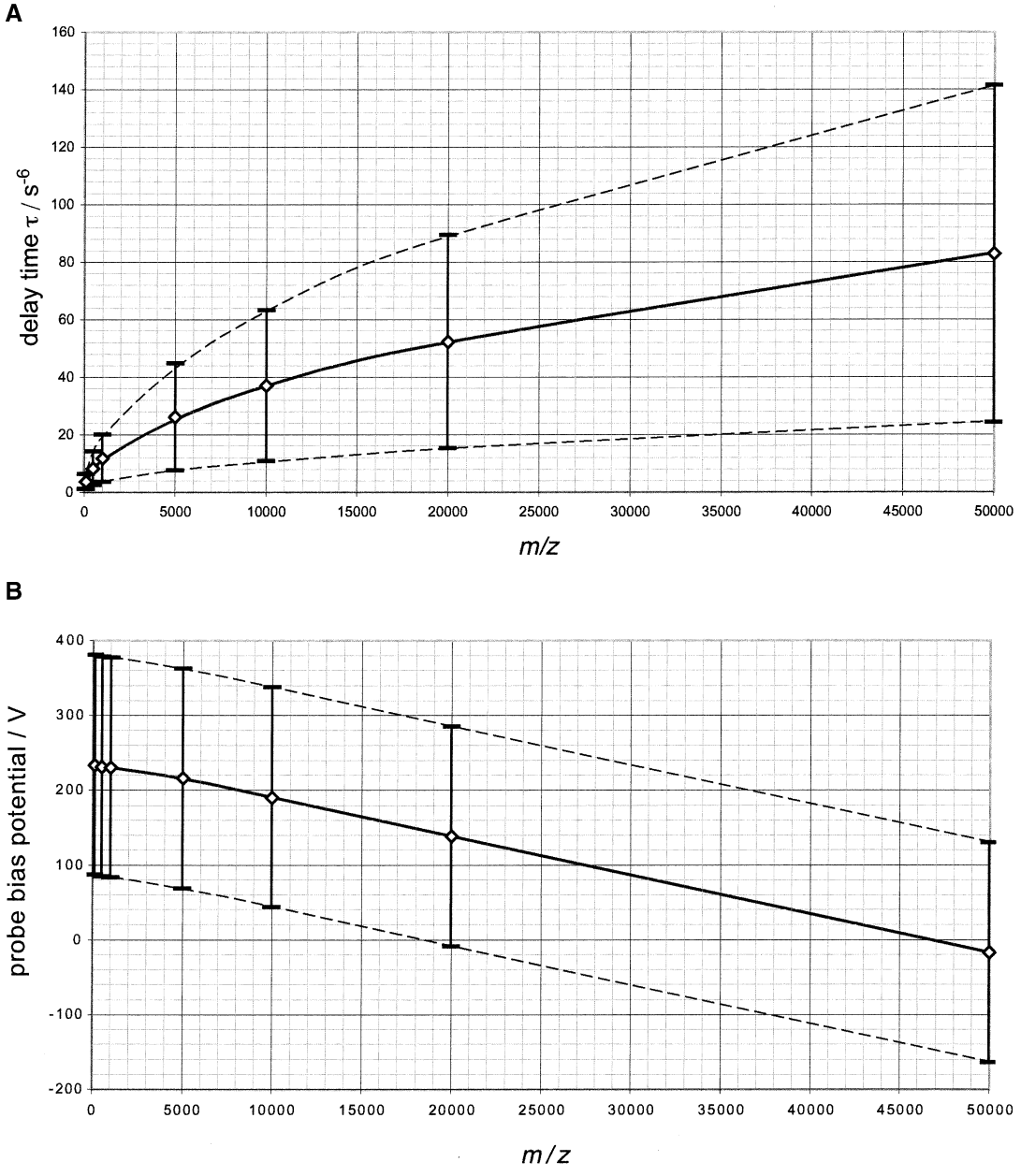

Fig. 5. Theoretical curves predicting, for a given *m/z*, the optimum: (a) delay time between laser firing and triggering of the push-out pulse and (b) probe bias voltage. The upper and lower dashed curves define the limits of the conditions imposed by geometric acceptance parameters of the detector.

from the ratio of the area of the shot to the area of the spot, with the knowledge that the sample preparation method typically allowed 50 shots to be made at the one location before the sample was depleted. The sensitivity decreased as molar mass increases. This may be attributed to the low efficiency of the detector used (see the following) and to the increasing "dilution" of the signal as mass increases. Ions were

Table 4
Estimation of detection limits

Sample	*m/z*	pmol in spot	fmol in shot area[a]	fmol in shot[b]	Shots req'd	fmol desorbed	S/N[c]	3 σ det limit (fmol)
Gramicidin S	1 163	1750	1167	23	20	467	51	~10
Melittin	2 844	700	467	9	30	280	59	~5
Insulin	5 374	700	467	9	60	560	23	~30
Myoglobin	17 000	480	320	6	200	1280	1	~1300

[a] Based on a spot area of 15 mm^2 and a shot area of 0.01 mm^2
[b] Based on typical 50 shots to deplete a shot location in a spot.
[c] Signal-to-noise ratio based on the signal height divided by an interval of 3 times the standard deviation of the baseline noise.

distributed over more digitizer samples as the peak width increased (see Fig. 4) and this was compounded by the increasing number of ^{13}C isotope combinations as the number of carbon atoms in the ions increased. The ITR digitizer used is not well suited to low ion count rates, owing to the baseline noise associated with this device. The sensitivity in the low fmol range is therefore reasonable for the arrangement used. Significant improvements would be expected if a more efficient detector were available and a pulse-counting digitizer was used.

3.5. Detector response

The gain of the MSP detector was measured by comparing the area of pulses observed at very low signal levels. The signal level was set so that pulses were not observed in a particular mass window in every shot. Under these conditions, the majority of pulses observed were for single ion arrival events for singly charged ions. The area of such pulses was expressed in coulombs and the gain of the detector in each mass range chosen was obtained by dividing by the charge of an electron. The distribution of gains displayed no trend with mass over the range *m/z* 200–17 000. The average gain was 3.1×10^6. The measured modes of the gain distributions ($/10^6$) were 1.3, 1.7, 1.3, 1.7, respectively, for ions at *m/z* ~200, ~1100, ~5700, and ~17 000. This is a good gain for a single plate device and a narrow pulse width was obtained (measured to be 800 $\pm$ 50 ps). The independence of the gain with respect to mass was not expected. In electron multiplier devices such as the MSP or the microchannel plate (MCP) detectors gain usually decreases significantly as *m/z* increases [10]. Recent investigations of the efficiencies of MCP detectors indicated that, for large biomolecular ions, there is a rapid fall in detector efficiency as ion velocity decreases [11]. The efficiency was found to be proportional to mass $\times$ velocity^4 or, when velocity is proportional to $(m/z)^{-0.5}$, efficiency for singly charged ions is inversely proportional to mass. A plausible explanation for constant gain is that the secondary electron emission efficiency is low even at low mass. If the most probable number of secondary electrons emitted is one or zero at low *m/z* then, as *m/z* increases, proportionately more ion arrival events generate no secondary electrons. Thus fewer pulses will be observed but most will be from single electron emission and they will indicate a consistent gain. Therefore the sensitivity falls with increasing *m/z* due to decreasing detector efficiency.

3.6 Pulsed focusing of source

The sensitivity of the detector used in the current version of the instrument is likely to be very low at high mass, as previously discussed. This combines unfavourably with the decreasing signal to noise ratio that is expected as ions become spread through more ITR samples due to increasing width of the peaks and isotopic distributions. For these reasons it was only possible to observe signals above *m/z* 10 000 with difficulty. A pulsed lens was designed to increase the number of high *m/z* ions reaching the detector [18]. The lens was pulsed so that ions were accelerated in the desorption direction a few microseconds after the

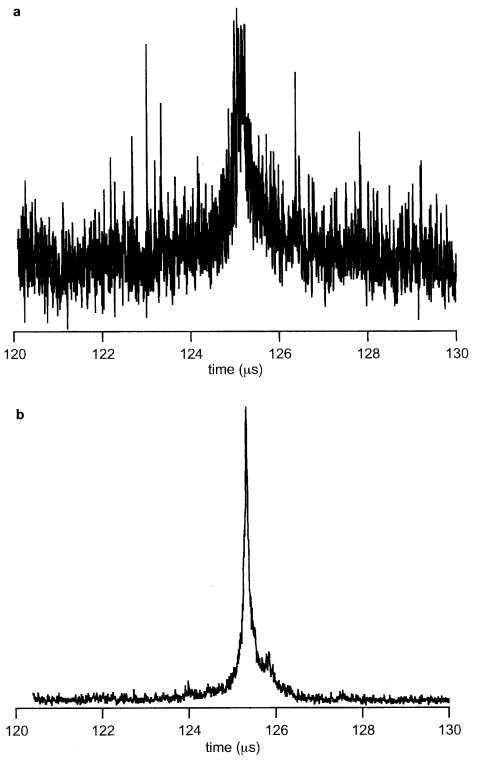

Fig. 6. Signals obtained for myoglobin (a) without the pulsed lens and (b) with the pulsed lens (delay 8 μs, amplitude 92 V).

laser fired. Similarly to delayed extraction, there is a correlation between the position of ions and their desorption velocities. The pulsed lens serves to apply maximum acceleration to the ions with the lowest desorption velocity and kinetic energy. In experiments the energy spread of the desorbing ions was thus decreased and the trajectories of the ions in drift regions of the TOF mass analyzer were less divergent. The lens simultaneously corrected for divergence of ions from the desorption axis, to increase the number ion ions sampled by the orthogonal accelerator. For ions with *m/z* 3000–6000 the lens increased the signal by a factor of about 20. A loss of resolution was apparent and this is attributed to the direction-focusing action of the lens leading to a larger velocity spread in the TOF direction. The signal for myoglobin was greatly increased as can be seen in Fig. 6. A refined design for the pulsed lens is under investigation and will be described in a future publication if it is successful.

4. Conclusion

A small and relatively simple 20 kV MALDI oa-TOF mass spectrometer has been constructed and shown to deliver resolution of ~8000 (FWHM). Correct orientation of the rectangular repeat cell grids was crucial in delivering this resolution. Calibration was very linear (TOF versus $[m/z]^{0.5}$) and the mass accuracy (external calibration over several days) was within expected limits of power supply drift and jitter, being considerably less than 100 ppm (standard deviation of mass error). Improvements in this can be expected if jitter in the timing electronics currently used is reduced. Sensitivity is estimated to be in the low fmol range below *m/z* 6000, degrading to the pmol range at *m/z* 17000. The sensitivity is limited, apparently, by the low efficiency of the detector (decreases further with increasing *m/z*) and the increasing energy spread of ions as *m/z* increases. A pulsed lens has been shown to improve the sensitivity of the mass spectrometer at high *m/z*.

Acknowledgements

The continuing funding of the Australian Research Council is gratefully acknowledged. El-Mul Technologies (Yavne, Israel) are thanked for supplying a MSP plate for evaluation. Mark Lewin is thanked for upgrading the SIMTOF program to facilitate the simulation of peak shape data presented in this article.

References

[1] M. Guilhaus, D. Selby, V. Mlynski, Mass Spectrom. Rev. 19 (2000) 65.
[2] I. V. Chernushevich, W. Ens, K. G. Standing, Anal. Chem. 71 (1999) 452A.
[3] J. H. J. Dawson, M. Guilhaus, Rapid Commun. Mass Spectrom. 3 (1989) 155.
[4] J. Coles, M. Guilhaus, Trends Anal. Chem. 12 (1993) 203.
[5] M. Karas, D. Bachmann, U. Bahr, F. Hillenkamp, Int. J. Mass Spectrom. Ion Processes 78 (1987) 53.
[6] R. G. Dworschak, W. Ens, V. Spicer, K. G. Standing, A. V. Verentchikov, in Proceedings of the 43rd ASMS Conference on Mass Spectrometry and Allied Topics, Atlanta, GA, 21–26 May 1995, p. 1219.

[7] V. Mlynski, M. Guilhaus, Rapid Commun. Mass Spectrom. 10 (1996) 1524.
[8] M. L. Vestal, P. Juhasz, S. A. Martin, Rapid Commun. Mass Spectrom. 9 (1995) 1044.
[9] J. J. Lennon, R. S. Brown, in Proceedings of the 42nd ASMS Conference on Mass Spectrometry and Allied Topics, Chicago, IL, 29 May–3 June 1994, p. 501.
[10] R. J. Beuhler, L. Friedman, Nucl. Instrum. Methods 170 (1980) 309.
[11] G. Westmacott, M. Frank, S. E. Labov, W. H. Benner, Rapid Commun. Mass Spectrom. 14 (2000) 1854.
[12] A. Shevchenko, A. Loboda, A. Shevchenko, W. Ens, K. G. Standing, Anal. Chem. 72 (2000) 2132.
[13] R. H. Bateman, R. S. Bordoli, A. J. Gilbert, J. B. Hoyes, H. R. Morris, in Proceeding of the 44th ASMS Conference in Mass Spectrometry and Allied Topics, Portland, OR 12–16 May 1996, p. 796.
[14] A. N. Krutchinsky, I. V. Chernushevich, V. L. Spicer, W. Ens, K. G. Standing, J. Am. Soc. Mass Spectrom. 9 (1998) 569.
[15] A. N. Krutchinsky, A. V. Loboda, V. L. Spicer, R. Dworschak, W. Ens, K. G. Standing, Rapid Commun. Mass Spectrom. 12 (1998) 508.
[16] D. Selby, V. Mlynski, M. Guilhaus, Int. J. Mass Spectrom. 206 (2001) 201.
[17] D. S. Selby, V. Mlynski, M. Guilhaus, Rapid Commun. Mass Spectrom. 14 (2000) 616.
[18] M. Guilhaus, M. J. Lewin, Australian Provisional Patent Application No. PQ9636, 2000.
[19] R. Naaman, Z. Vager, Rev. Sci. Instrum. 67 (1996) 3332.
[20] R. B. Opsal, K. G. Owens, J. P. Reilly, Anal. Chem. 75 (1985) 1884.
[21] J. N. Coles, M. Guilhaus, J. Am. Soc. Mass Spectrom. 5 (1994) 772.
[22] D. S. Selby, M. Guilhaus, unpublished.
[23] A. A. Puretzky, D. B. Geohegan, G. B. Hurst, M. V. Buchanan, Phys. Rev. Lett. 83 (1999) 444.
[24] Y. Pan, R. J. Cotter, Org. Mass Spectrom. 27 (1992) 3.
[25] B. Spengler, R. J. Cotter, Anal. Chem. 62 (1990) 793.
[26] R. G. Dworschak, V. Spicer, W. Ens, K. G. Standing, in Proceedings of the 46th ASMS Conference on Mass Spectrometry and Allied Topics, Orlando, FL, 31 May–4 June 1998, p. 932.
[27] M. Glückmann, M. Karas, J. Mass Spectrom. 34 (1999) 467.